2024 Design, Automation & Test in Europe Conference (DATE 2024)

Design Automation for Organs-on-Chip

Maria Emmerich,[1] Philipp Ebner,[2] and Robert Wille[1,3]

[1] Technical University of Munich (TUM), Arcisstrasse 21, 80333 Munich, Germany
[2] Johannes Kepler University Linz (JKU), Altenberger Strasse 69, 4040 Linz, Austria
[3] Software Competence Center Hagenberg GmbH (SCCH), Softwarepark 32a, 4232 Hagenberg, Austria
maria.emmerich@tum.de, philipp.ebner@jku.at, robert.wille@tum.de
https://www.cda.cit.tum.de/research/microfluidics/

***Abstract*—*Organs-on-Chips* (OoCs) are testing platforms for the pharmaceutical, cosmetic, and chemical industries. They are composed of miniaturized organ tissues (so-called organ modules) that are connected via a microfluidic channel network and, by this, emulate human or other animal physiology on a miniaturized chip. The design of those chips, however, requires a sophisticated orchestration of numerous aspects, such as the size of organ modules, the required shear stress on membranes, the dimensions and geometry of channels, pump pressures, etc. Mastering all this constitutes a non-trivial design task for which, unfortunately, no automatic support exists yet. In this work, we propose a first design automation solution for OoCs. To this end, we review the respective design steps and formalize a corresponding design specification from it. Based on that, we then propose an automatic method which generates a design of the desired device. Evaluations (inspired by real-world use cases and confirmed by CFD simulations) demonstrate the applicability and validity of the proposed approach.**

***Index Terms*—microfluidics, micro physiological system, organ-on-chip, physiological perfusion, shear stress, multi-organ**

I. Introduction

Pharmaceutical, cosmetic, and chemical industries heavily rely on testing platforms for the development of compounds. For this purpose, they frequently fall back to animal studies—with all its ethical consequences. At the same time, more and more regions restrict the use of animal testing (e.g., in the European Union with the Directive 2010/63/EU, or in the US with the FD&C Act). Moreover, 85 % of pharmaceuticals fail when they are translated from animal studies to clinical trials [1] as a result of unanticipated toxic side effects since animal models differ from the human organism [2]. Consequently, there is a substantial need for alternative testing platforms.

Organs-on-Chip (OoC) platforms provide the most promising solution to this problem [3], [4]. They hold miniaturized tissues (called *organ modules*) that simulate key aspects of human or other animal organs and connect them in a physiologically relevant fashion through a *membrane* to a microfluidic network containing a *circulating fluid*. Each organ module mimics key features of the represented organism. The circulating fluid supplies the organs with nutrients, removes waste, and transports messenger molecules that allow inter-organ communication. By this, OoCs provide the missing link between simple, ordinary cell culture approaches, which are the basis for identifying pharmaceutical compounds, and clinical trials by supplementing or replacing animal studies.

However, the design of corresponding OoCs is not a trivial task and requires a sophisticated orchestration of numerous aspects, such as the size and scale of organ modules, the required shear stress on membranes, the dimensions and geometry of channels, pump pressures, etc. These aspects are correlated, and even slight changes can affect the whole system. Moreover, because of the various applications of OoC systems, the testing of compounds, e.g., for patient-specific applications (testing a treatment on a platform with patient-derived tissues prior to treatment of the patient) requires frequent redesigns—leading to severe design and fabrication loops. Considering that currently design automation for microfluidics focuses only on other topics such as meander routing [5], [6], microfluidic droplet networks [7], [8], gradient generators [9], etc. and that the design of OoCs is still conducted manually thus far, this leaves a tedious, error-prone, and costly task that urgently requires automation.

In this work, we propose a design automation solution for OoCs to solve the laborious task described above. To this end, we review the respective design steps and formalize the corresponding constraints in terms of a formal specification. Based on that, we then propose an automatic method that realizes the desired OoC. Evaluations considering a total of 288 OoC instances (most of them inspired by real-world examples) demonstrate the applicability of the proposed approach and confirm that, in the vast majority of cases, the proposed method is capable of generating the desired designs.

The remainder of this work is structured as follows: First, we review OoCs and their design—providing the basis and motivation for this work. Afterwards, Section III introduces the proposed design automation approach. Section IV summarizes the conducted evaluations. Finally, Section V concludes this paper.

II. Background and Motivation

In this section, we first review the concept of *Organs-on-Chip* (OoC). Afterwards, we discuss the design of corresponding devices and the current shortcomings of this process—providing the motivation of this work.

A. Organs-on-Chip

The concept of an OoC is to model human or other animal physiology on a miniaturized chip. For this to work, it is essential to include organ tissues to represent the desired organs and to connect them in a relevant way. To this end, any OoC is composed of three main components: the organ modules that hold the organ tissues, the circulating fluid that connects the organ modules, and the membranes that define the connection between organ modules and circulating fluid. More precisely:

Organ modules are tissue constructs that represent miniaturized organs. They try to replicate the functions and interactions inside an organism (in vivo) and can be 3D-printed [10], lab-grown [11], or collected from specimens such as tumor tissue [12]. For these tissues to stay alive and grow, they need to be supplied with nutrients like glucose and oxygen. Therefore, organ modules constitute a fundamental part of every OoC device. They are connected to an inlet and an outlet to ensure media replenishment and a continuous flow [13]. Eventually, this results in a simplified version of how cells in the human body are supplied with oxygen and nutrients.

However, while culturing organs in a single tissue chip can provide insights into the mechanisms within that single organ, the intra-body communication and response to disease, injury, and therapy can only be investigated if a *combination* of organ modules is considered [3]. Hence, to properly emulate (parts of) larger organisms, multiple organ modules are realized within an OoC. Since these organ modules communicate through cytokines (messenger molecules that allow inter-organ communication), a corresponding and dedicated *circulating fluid* is needed. This circulating fluid does not only provide the required nutrients but also takes and transports these cytokines from and between the organ modules.

979-8-3503-4859-0/DATE24/© 2024 EDAA

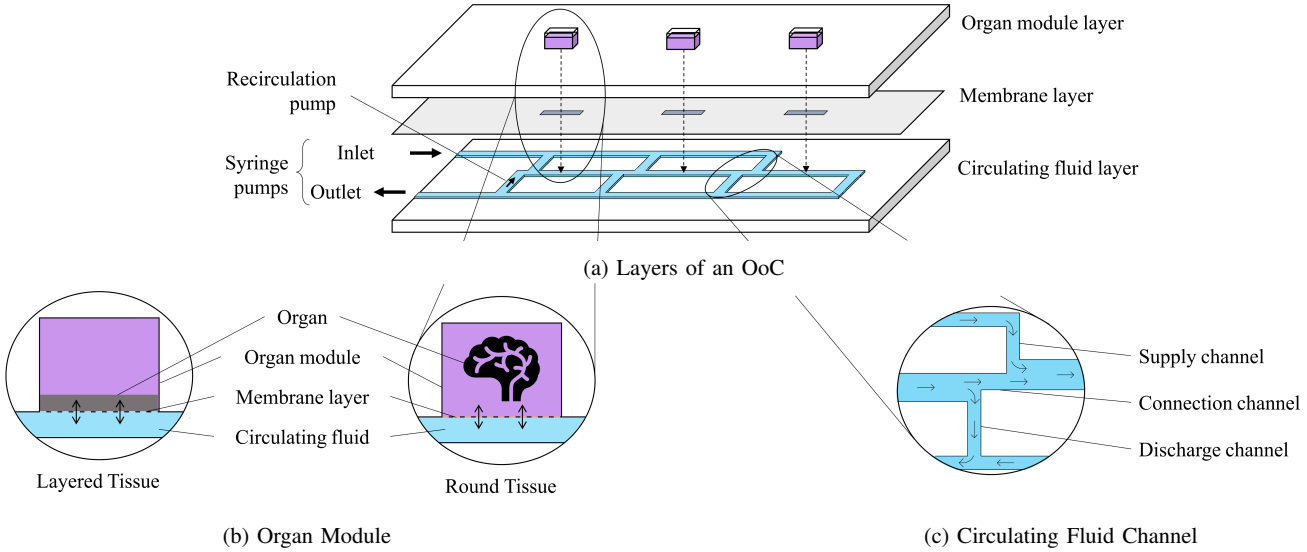

(a) Layers of an OoC

(b) Organ Module

(c) Circulating Fluid Channel

Fig. 1: OoC Layout

Finally, to couple the organ modules with the circulating fluid, a *membrane* is used that simulates the endothelium, i.e., the inner lining of blood and lymph vessels. This results in a model that emulates the organ tissue-blood barrier and is usually achieved by seeding the membrane with endothelial cells. This results in realistic drug absorption, distribution, metabolism, excretion, and toxicity [3], [14].

Overall, this leads to OoCs that realize the interactions between organ modules either through (1) distinctive predefined systems [4], [15] (that are static and designed for an exact combination of organs) or (2) plug-and-play connection systems [3], [16], [17] (that are more flexible and can realize different combinations of organs).

B. Design of Organs-on-Chip

At a first glance, the design of OoCs may look simple: Organ modules (for which several solutions are fabricated by researchers; see, e.g., [4], [18], [19]) have to be taken and connected through a circulating fluid. However, the realization of (1) the correspondingly needed interplay between different organ modules, (2) a proper microfluidic network for the circulating fluid, and (3) the membranes for an appropriate connection between both is a non-trivial task. In the following, we briefly review the correspondingly needed steps. To this end, we follow the main structure of OoCs as sketched in Fig. 1a and composed of corresponding layers for the organ modules, the membrane, and the circulating fluid.

1) Organ Modules: First, the respective required modules need to be defined. The corresponding organ tissues inside them can be one of two types (as sketched in Fig. 1b): A layered tissue or a round tissue. The former consists of cell layers that grow directly on the epithelial membrane. Typical examples include barrier tissues such as the lung or the skin. Round tissues consist of cell layers that are formed like a spheroid or sphere and are suspended in fluid. Typical examples include tumor tissues, but other organs like brain tissue can also be represented by spheres.

In order to properly design a combination of organ modules, the respective sizes of the modules obviously have to be proportional (since their relationship to each other and their impact on the system should be replicated the same way they interact in the represented organism [14]). At the same time, the organ size is restricted to a width of 500 µm since lab-grown or tissue-engineered organs lack vascularization (growth of blood vessels into a tissue) [11], [20], [21]. A larger tissue would, therefore, lead to a lack of oxygen as well as nutrients and, hence, to necrotic (i.e., dead) tissue in the organ center. Defining the size of all organ modules also directly affects the design of the remaining two layers of an OoC.

2) Membranes: The membrane layer connects organ modules to the circulating fluid and, hence, is obviously placed between the other two layers (cf. Fig. 1a). The membranes are usually seeded with endothelial cells to simulate a vascular system and realize the cytokine and molecule exchange between each organ module and the circulating fluid. The sizes of the membranes obviously depend on the sizes of the respective modules and have to be designed accordingly. Moreover, the membrane, or, more precisely, the endothelial cells growing on the membrane (blood vessel model), need to be exposed to a dedicated shear stress. That is, the tangential force that is applied to the endothelial layer should be low enough to not wash away the endothelial cells that are growing on the membrane. At the same time, it should replicate the shear stress of the represented organism to prevent dedifferentiation [22], i.e., the loss of cellular characteristics [23]. This, in turn, also affects, e.g., the required flow rate of the circulating fluid in the remaining layer.

3) Circulating Fluid Network: Finally, the circulating fluid connects the different organ modules and, by this, allows for the needed inter-organ communication. This is realized by a dedicated microfluidic network, as sketched in the bottom of Fig. 1a as well as in Fig. 1c. Here, a *supply channel* is realized, which (through the inlet) introduces fresh fluid and, by this, new nutrients into the system (and, hence, to the organ modules). Vice versa, a *discharge channel* is realized which (through the outlet) removes fluid, including any produced waste products, from the system. Both, the supply channel and the discharge channel have to employ the same flow rate (realized by the pumps) in order to keep the system at equilibrium. Additionally, a recirculation pump ensures that part of the discharge fluid is redirected back into organ modules. Finally, a *connection channel* directly connects one organ module with the next organ module.

With that, the entire design of this network is key to achieve the desired physiological inter-organ communication. More precisely, the dimensions and geometry of the channels as well as the realization of the respective branching eventually regulate the flow rates of each channel. This is turn realizes the physiological perfusion and, by this, the rate of blood flow (emulated by the circulating fluid within

this network) through the tissue. Properly defining those flow rates is required to ensure that, e.g., organs with a lower perfusion are exposed to a lower volumetric flow rate, while organs with high perfusion like the liver are exposed to a larger flow rate. This, together with the size of the modules and the respective required shear stress to be realized on the membranes, requires a careful design of the entire network.

Overall, in order to properly design an entire OoC, a sophisticated orchestration of numerous aspects is required (starting from the specification of organ modules and membranes over the required/allowed shear stress acting on the membranes towards dedicated dimensions and geometry of channels, pump pressures, etc. for the microfluidic network realizing the circulating fluid layer). Eventually, this results in various constraints that need to be considered when generating a corresponding design. Resolving all these linked aspects is a complex task that is mainly conducted manually thus far. Accordingly, the design of corresponding devices still remains a tedious, error-prone, and costly task that urgently requires automation.

III. Automatic Design for Organs-on-Chip

In this section, we propose an *automatic* solution which solves the tasks reviewed above. To this end, we first derive a *specification* incorporating the numerous aspects to be considered in a formal fashion. Afterwards, we describe the proposed *design automation* method that is used to generate the desired OoC from this specification.

A. Determining the Specification of the Desired OoC

To determine the specification of the desired OoC, the aspects that were reviewed in the previous section need to be formalized. Again, this includes the specification of the organ modules and membranes, the required/allowed shear stress acting on the membranes, and the physiological perfusion of the organ modules.

1) Specification of the Organ Modules: First, the organ modules which shall be used need to be defined. This includes the specification of its *tissue type* and *size*. In general, two main organ types are used in OoCs: round tissues and layered tissues (as reviewed above and shown in Fig. 1b). Determining the tissue type is necessary for the later determination of the size of the organ basin. If only layered tissues are used, the channel width that is equal to the module width is set to $1\,\mathrm{mm}$. If, instead, at least one round tissue is included in the OoC, its radius r defines the module size and, hence, the circulating fluid channel width. More precisely, then, the organ module width and length are equal to $4 \times r$ where $r \leq 250\,\mu\mathrm{m}$ [21].

Afterwards, the sizes of the organ modules need to be adjusted in relation to each other so that they indeed represent a scaled-down version of the considered organism. This can be realized by linearly scaling each organ, which results in the same mass (and volume) relation as in the represented organism. More precisely, when the mass of the complete scaled down organism M_b [kg] ("total mass of the miniaturized organism") is unknown, it can be determined by specifying the desired mass of the miniaturized organ module M_m [kg] using

$$M_b = \frac{M_m \times M_h}{M_{Tissue}}, \tag{1}$$

where M_h [kg] is the mass of a reference standard human, and M_{Tissue} [kg] is the reference mass of the tissue in the reference standard human. Based on that, the weight of all remaining organ modules can be determined using

$$M_m = \frac{M_{Tissue} \times M_b}{M_h}. \tag{2}$$

Together, organ type and mass (and volume) define the module size and also influence the specification of the channel width and geometry of the microfluidic network.

Example 1. *A typical organ module in an OoC is a liver module. The size of the liver of a standard human male (*$70\,\mathrm{kg}$*) is* $1\,\mathrm{kg}$ *[24]. In a miniaturized liver-on-chip that simulates the liver of an organism with a weight of* $1 \times 10^{-6}\,\mathrm{kg}$*, the liver organoid would have a mass of approx.* $1.42 \times 10^{-8}\,\mathrm{kg}$*. This results in a organ module length of* $89\,\mu\mathrm{m}$ *at a width of* $1\,\mathrm{mm}$ *and tissue height of* $150\,\mu\mathrm{m}$*.*

2) Shear Stress on Membrane: The endothelial layer that separates the organ modules from the circulating blood surrogate needs to be exposed to continuous shear stress τ [Pa] that is low enough to not wash away the endothelial cells growing on the membrane. At the same time, it should replicate the shear stress of the represented organism, which should be strong enough to prevent dedifferentiation (loss of cellular characteristics). According to [23], this means the shear stress should be between $1\,\mathrm{Pa}$ to $2\,\mathrm{Pa}$.

To make sure the shear stress remains within this range, it can be controlled by the flow rate

$$Q = \frac{\tau \times w_{channel} \times h_{channel}^2}{6 \times \mu}, \tag{3}$$

where $w_{channel}$ [m] is the channel width of the channel that is connected to the organ module, $h_{channel}$ [m] its channel height, and μ [Pa s] is the dynamic viscosity of the circulating fluid [25]. The flow rate can later be experimentally controlled and is an output of the presented method.

3) Physiological Perfusion for Organ Communication: The physiological perfusion plays a significant role in the physiological relevance of the model. It describes the rate of blood flow through a tissue. In the OoC model, it is represented by a physiological perfusion factor $perf$ that resembles the fraction of circulating fluid that is exchanged between the organ modules. The higher the perfusion, the higher the exposure of the organ module to the circulating fluid. This percentage is determined by

$$perf = \frac{Q_{organblood}}{Q_{totalblood}} \times \frac{V_{circ.fluid}}{V_{blood}}, \tag{4}$$

where $Q_{organblood}$ [m^3/s] is the standard blood flow through the organ, $Q_{totalblood}$ [m^3/s] is the standard cardiac blood throughput, $V_{circ.fluid}$ [m^3] is the total volume of the circulating fluid flow, and V_{blood} [m^3] is the scaled down blood volume of a standard human male proportional to the organ sizes on the OoC.

It also includes the dilution of the communication molecules due to the larger circulating fluid volume compared to the blood volume. In the current configuration, the dilution factor $\frac{V_{circ.fluid}}{V_{blood}}$ is set to 2. The channel branching (cf. Fig. 1c) allows to balance the flow rate to fulfill the requirements for shear stress as well as the physiological perfusion between organ modules.

Example 2. *Consider again the liver-on-chip module from above. The reported physiological perfusion of the liver in a standard human male is* $1450\,\mathrm{mL\,min^{-1}}$*. Together with a dilution factor of* 2*, this results in a volume exchange of* $55.4\,\%$ *for the liver module. This percentage is then multiplied with the flow rate below the organ modules—resulting in the flow rate required in the connection channel [24]. The flow rate of the discharge channel is the remaining flow* $(1 - perf) \times Q$*, which results in* $44.6\,\% \times Q$ *and is equal to the flow rate of the supply channel.*

Utilizing the equations and constraints from above results in a precise specification for the entire OoC design. Their orchestration, including the relation between organ modules and the flow rates for the circulating fluid network, then needs to be realized. An automated solution for this is described in the next section.

B. Realization of the Specification

Using the formal specification introduced above, an OoC design can be realized in an automatic fashion. For the organ modules and the size of the membranes, this can easily be accomplished by employing Eq. 1 and Eq. 2. In contrast, the realization of the microfluidic network for the circulating fluid requires some more steps in order to ensure that additional aspects such as pressure gradients and resistances are accounted for. Here, the entire geometry of the network as well as dimensions of the single channels need to be created so that the correspondingly needed flow rates are realized. To this end, the following four steps are performed:

- *Initialization:* Determine the required flow rate for all channels.
- *Pressure Correction:* Match the pressure gradient, flow rate, and resistance of each channel.
- *Meander Insertion:* Design the supply and discharge channels such that they implement the desired resistance by adjusting their lengths.
- *Offset Correction:* Adjust the offsets of the supply and discharge channels (cf. Fig. 2) such that there is enough space to actually place all channels.

The latter three steps are carried out until no further pressure correction is necessary. The result is a valid OoC chip design as well as flow rate settings for the pumps. In the following, these steps are described in detail:

1) Initialization: First, the flow rates in all channels (cf. Fig. 2) are determined. For each organ module M_i, the required flow rate Q_i^M can be determined by Eq. 3. The flow rate Q_i^c of the connection between modules depends on the perfusion (cf. Eq. 4) and can be determined by $Q_i^c = perf \times Q_i^M$. The remaining flow rates can be determined by applying *Kirchhoff's current law* [26]: For each node (i.e., where multiple channels meet), the sum of the incoming flow rates equals the sum of the exiting flow. These nodes and the flow rates are illustrated for two modules in Fig. 2. Consequently, the relations

$$\begin{aligned} Q_i^s &= Q_i^M - Q_i^c, \\ Q_i^{sf} &= Q_{i+1}^{sf} + Q_i^s, \\ Q_i^d &= Q_i^M - Q_{i+1}^c, \text{ and} \\ Q_i^{dd} &= Q_{i+1}^{dd} + Q_i^d \end{aligned} \tag{5}$$

allow to determine the remaining flow rates. Then, the required flow rates for the inlet and outlet pumps (cf. Fig. 1a) are equal to the flow rates of the supply feed and discharge drain channel of the first module, i.e., Q_0^{sf} and Q_0^{dd}. Conversely, the flow rate of the connection channel Q_0^c in front of the first module defines the flow rate of the recirculation pump.

Second, the dimensions for each channel are fixed, i.e., the width w, height h, and length l are assigned. The module channel dimensions can be determined as described in Section III-A. The other channels can be freely sized. However, a reasonable choice is to use a uniform channel height throughout the chip. Additionally, the supply feed and discharge drain (horizontal channels) can be set to the same width as the module channel, while the vertical supply and discharge channels (cf. Fig. 2) should have a smaller diameter (e.g., $\frac{h}{w} = \frac{2}{3}$).

Finally, the channel resistances are computed. The resistance R of a rectangular channel is determined by the width w and height h of its cross-section, as well as its length l [27]. If $h \leq w$, and given the viscosity μ of the fluid, then a channel implements the resistance[1]

$$R = \frac{12\mu l}{1 - 0.63(\frac{h}{w})} \frac{1}{h^3 w}. \tag{6}$$

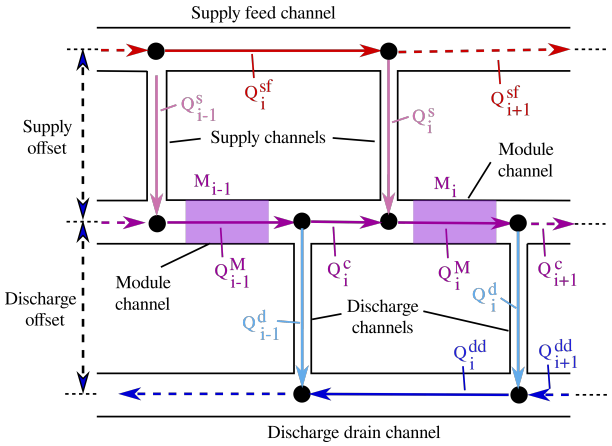

Fig. 2: Flow rate nodes

2) Pressure Correction: Using the information from the previous step, the pressure gradients can be computed for every channel by employing the *Hagen-Poiseuille* equation [26], i.e.,

$$\Delta P = RQ, \tag{7}$$

where ΔP is the difference in pressure between two channel ends, R is the channel's resistance, and Q is the flow rate in the channel. However, the channels may still violate *Kirchhoff's voltage law* [26] since, along any closed cycle of channels, the sum of oriented pressure gradients must be zero. To correct this violation, the pressure gradients of each module's vertical supply and discharge channels are manipulated by changing the channels' lengths until Kirchhoff's voltage law is satisfied.

This is illustrated in Fig. 3. More precisely, starting with the last organ module and iterating backwards, the supply and discharge channels are adjusted such that the sum of pressure gradients around each cycle is zero, i.e.,

$$\begin{aligned} \Delta P_i^s &= \Delta P_{i+1}^{s\prime} \\ \Delta P_i^d &= \Delta P_{i+1}^{d\prime}, \end{aligned} \tag{8}$$

where ΔP_i^s, ΔP_i^d are the pressure gradients along the supply and discharge channels of the module, and $\Delta P_{i+1}^{s\prime}$, $\Delta P_{i+1}^{d\prime}$ complete the cycle as indicated in Fig. 3 (marked by red arrows for the supply cycle and blue arrows for the discharge cycle). Such a pressure adjustment can be achieved in two ways:

1) If the pressure gradient needs to be larger, increase the channel's length l_i^s or l_i^d and, therefore, its resistance and pressure gradient.
2) If the pressure gradient needs to be smaller, it may not be possible to shorten the channel length in the same way. Instead, make all channels of the succeeding modules longer such that the voltage law is satisfied in the same way.

By employing this procedure, it is ensured that the supply and discharge channels strictly increase and, thus, pressure correction can indeed be applied.

[1]This is an approximation for $\frac{h}{w} \to 0$, i.e., wide channels, which is the common case.

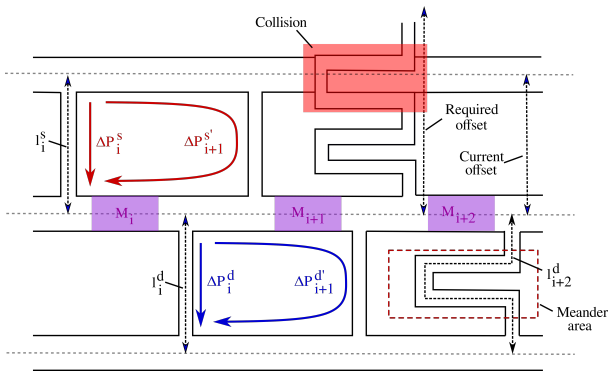

Fig. 3: Pressure gradient cycles and meanders

3) Meander Insertion: The next task is to physically design the channels such that they can accommodate the additional length from the previous step. To this end, so-called *meander channels* [5] are used. Fig. 3 illustrates how meanders are used to increase the channel length until the required length is achieved.

4) Offset Correction: Finally, it is not guaranteed that the meanders that have been created in the previous step will fit into the space between the organ modules and supply feed/discharge drain channel—possibly creating a collision as illustrated for the upper meander in Fig. 3 (highlighted red). If this is the case, the supply and discharge offsets need to be adjusted such that every meander has enough space to fit in. However, after this correction, there may be supply/discharge channels that are too short and, therefore, their length and pressure gradient change, after which further pressure correction is needed. Hence, these three steps are carried out until no further pressure correction is necessary.

Overall, after completing the procedure described above, an OoC design results that consists of organ modules with properly dimensioned tissue sizes and a microfluidic network for the circulating fluid realizing the desired flow and perfusion rate. The open-source software implementation is available at https://github.com/cda-tum/mmft-ooc-designer.

IV. Evaluation

In order to demonstrate the applicability and validity of the proposed design automation method for OoCs, we used the approach proposed above to automatically generate various OoC designs. To this end, different OoC use cases have been considered, from which a corresponding specification has been derived as described in Section III-A. Based on that, a design has been generated as described in Section III-B. In order to validate whether the resulting designs work as intended, *Computational Fluid Dynamics* (CFD) simulations [28], [29] have been conducted.

As use cases, we considered four examples of OoCs inspired by real-world examples with predefined organ arrangements and organ tissue types. This includes combinations of a barrier tissue like the lung or the gastro-intestinal tract for drug uptake [4] with the liver, which plays a major role in the body's metabolism [30] and the brain, as it differs the most between humans and other animals [11]. For a combination of lung, liver, and brain the *male_simple* and *female_simple* use cases represent the respective sexes of an OoC. The *male_gi_tract* use case uses the gastro-intestinal tract as a barrier tissue (instead of the lung). Finally, the *male_kidney* use case additionally includes the kidney, allowing for the investigation of potential side effects on this organ [31]. Furthermore, four generic and larger use cases with liver tissue were considered in order to demonstrate scalability (denoted by *generic1* to *generic4*). For each

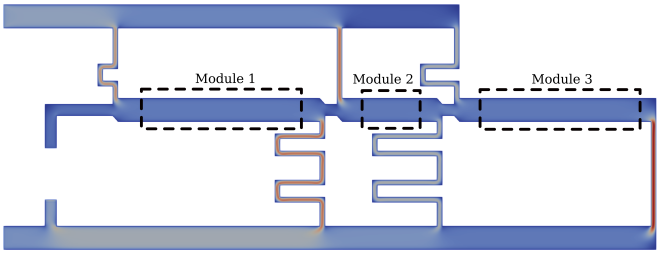

Fig. 4: CFD simulation for the *male_simple* chip

of these use cases, a variation of certain parameters has been applied, i.e., each basic OoC use case was instantiated for several viscosity values $\mu \in \{7.2 \times 10^{-4}, 9.3 \times 10^{-4}, 1.1 \times 10^{-3}\}[\mathrm{Pa\,s}]$ [32], shear stress values $\tau \in \{12 \times 10^{-1}, 15 \times 10^{-1}, 20 \times 10^{-1}\}[\mathrm{Pa}]$ [33], and spacing values (minimum distance between channels) $\{0.5 \times 10^{-3}, 1 \times 10^{-3}, 1.5 \times 10^{-3}\}[\mathrm{m}]$. In total, this led to 288 OoC designs which have been generated.

Afterwards, the resulting designs have been validated using the CFD simulator OpenFOAM [29]. As a representative, the resulting design (as well as simulation result) for an instance of the *male_simple* use case is shown in Fig. 4. Here, the color gradient illustrates the fluid velocities, which shows that the velocities and, therefore, also the flow rates are approximately the same in each module channel (marked by boxes). More precisely, the measured flow rates for modules 1, 2, and 3 are 7.66, 7.92, and 7.88 $[10^{-9}\mathrm{m}^3/\mathrm{s}]$, respectively, whereas the chip was intended to have a flow rate of 7.81 $[10^{-9}\mathrm{m}^3/\mathrm{s}]$ in all modules—resulting in a deviation between the specification and the resulting design of 1.90%, 1.41%, and 0.86%, respectively. Conversely, the measured perfusion rates for each module deviate from the intended values by 1.95%, 0.09%, and 1.87%. Since those deviations are negligible and way below typical tolerances applied in microfluidics [34], this confirms that the design that has been (automatically) created by the proposed approach works as intended.

For all remaining instances, we summarized the obtained results in Table I. Here, the first two columns provide the identifier of the use case as well as the respectively considered number of organ modules. Afterwards, the relative deviations (in %) in perfusion rates and module flow rates between the specification and the resulting design (as obtained by the CFD simulation) are provided (note that we aggregated these values for all instances and provide the average deviation and the maximal, i.e., worst-case, deviation in Table I).

These results clearly show how accurately the proposed method realizes the desired OoC designs in most of the cases. Granted, there are a few single instances in which the deviation gets significant (e.g., for *generic3* with a deviation of up to 9.5% in the worst case). This is because, after all, for an efficient design automation method, simplifications such as using approximate formulas for certain physical quantities (e.g., Eq. 6) cannot be avoided (which is why every design should be simulated before further consideration). However, in the vast majority, the deviations are negligible. In fact, on average, the deviations are less than 3% (even including the worst cases)—which, again, is within the typical tolerances applied in microfluidics and, hence, more than acceptable for an automatically generated microfluidic design.This clearly confirms, on a broad spectrum of OoCs, that the proposed method is capable of (automatically) generating the desired designs.

V. Conclusion

In this work, we proposed an automated design approach for Organs-on-Chip. The approach masters the orchestration of numerous aspects such as the size of organ modules, the required shear stress

TABLE I: Summary of obtained results

Chip	Modules	Deviation [%] in perfusion		Deviation [%] in flow rate	
		avg	max	avg	max
male_simple	3	0.98	3.60	1.15	3.38
female_simple	3	0.85	2.91	1.17	2.77
male_gi_tract	3	1.16	6.90	0.80	1.99
male_kidney	4	1.46	8.50	1.56	5.77
generic1	5	2.60	7.63	1.86	5.56
generic2	6	1.15	6.49	1.47	6.23
generic3	7	1.63	9.56	2.19	6.32
generic4	8	1.44	7.95	2.15	6.36

on membranes, the dimensions and geometry of channels, pump pressures, etc., and, by this, substantially improves this design task, which, thus far, was executed manually. Eventually, the resulting method accounts for physiological parameters and automatically generates a corresponding microfluidic chip design. The applicability and validity of the generated designs have been evaluated using instances inspired by real-world use cases and CFD simulations, respectively. To the best of our knowledge, this is the first attempt towards design automation for OoCs, which is available at https://github.com/cda-tum/mmft-ooc-designer, and, by this, provides a fundamental basis for the further development of automatic design methods for OoCs.

ACKNOWLEDGMENT

This work has partially been supported by the FFG project AUTOMATE (project number: 890068) as well as by BMK, BMDW, and the State of Upper Austria in the frame of the COMET Programme managed by FFG.

REFERENCES

[1] I. W. Mak, N. Evaniew, and M. Ghert, "Lost in translation: animal models and clinical trials in cancer treatment," *American Journal of Translational Research*, vol. 6, no. 2, pp. 114–118, 2014.

[2] K. Viravaidya, A. Sin, and M. L. Shuler, "Development of a microscale cell culture analog to probe naphthalene toxicity," *Biotechnology Progress*, vol. 20, no. 1, pp. 316–323, 2008.

[3] K. Ronaldson-Bouchard, D. Teles, K. Yeager, D. N. Tavakol, Y. Zhao *et al.*, "A multi-organ chip with matured tissue niches linked by vascular flow," *Nature Biomedical Engineering*, vol. 6, no. 4, pp. 351–371, 2022.

[4] M. B. Esch, H. Ueno, D. R. Applegate, and M. L. Shuler, "Modular, pumpless body-on-a-chip platform for the co-culture of GI tract epithelium and 3d primary liver tissue," *Lab on a Chip*, vol. 16, no. 14, pp. 2719–2729, 2016.

[5] A. Grimmer, P. Frank, P. Ebner, S. Häfner, A. Richter *et al.*, "Meander designer: Automatically generating meander channel designs," *Micromachines*, vol. 9, no. 12, 2018.

[6] P. Ebner, G. Fink, and R. Wille, "Channel routing for microfluidic devices: A comprehensive and accessible design tool," *IEEE Transactions on Computer-Aided Design of Integrated Circuits and Systems*, vol. 42, no. 2, pp. 533–543.

[7] G. Fink, M. Hamidović, W. Haselmayr, and R. Wille, "Automatic design of droplet-based microfluidic ring networks," *Trans. on Computer-Aided Design of Integrated Circuits and Systems*, 2020.

[8] A. Grimmer, W. Haselmayr, and R. Wille, "Automatic droplet sequence generation for microfluidic networks with passive droplet routing," *Comput.-Aided Des. Integr. Circuits Syst.*, 2018.

[9] G. Fink, T. Mitteramskogler, M. A. Hintermüller, B. Jakoby, and R. Wille, "Automatic design of microfluidic gradient generators," *IEEE Access*, vol. 10, pp. 28 155–28 164, 2022.

[10] H.-G. Yi, H. Lee, and D.-W. Cho, "3D printing of organs-on-chips," *Bioengineering*, vol. 4, no. 4, p. 10, 2017.

[11] S. Kofman, N. Mohan, X. Sun, L. Ibric, E. Piermarini *et al.*, "Human mini brains and spinal cords in a dish: Modeling strategies, current challenges, and prospective advances," *Journal of Tissue Engineering*, vol. 13, p. 204173142211133, 2022.

[12] M. R. Haque, C. R. Wessel, D. D. Leary, C. Wang, A. Bhushan *et al.*, "Patient-derived pancreatic cancer-on-a-chip recapitulates the tumor microenvironment," *Microsystems & Nanoengineering*, vol. 8, no. 1, p. 36, 2022.

[13] K. Ronaldson-Bouchard and G. Vunjak-Novakovic, "Organs-on-a-chip: A fast track for engineered human tissues in drug development," *Cell Stem Cell*, vol. 22, no. 3, pp. 310–324, 2018.

[14] R. Prantil-Baun, R. Novak, D. Das, M. R. Somayaji, A. Przekwas *et al.*, "Physiologically based pharmacokinetic and pharmacodynamic analysis enabled by microfluidically linked organs-on-chips," *Annual Review of Pharmacology and Toxicology*, vol. 58, no. 1, pp. 37–64, 2018.

[15] Y. Baert, I. Ruetschle, W. Cools, A. Oehme, A. Lorenz *et al.*, "A multi-organ-chip co-culture of liver and testis equivalents: a first step toward a systemic male reprotoxicity model," *Human Reproduction*, vol. 35, no. 5, pp. 1029–1044, 2020.

[16] Y. S. Zhang, J. Aleman, S. R. Shin, T. Kilic, D. Kim *et al.*, "Multisensor-integrated organs-on-chips platform for automated and continual in situ monitoring of organoid behaviors," *Proceedings of the National Academy of Sciences*, vol. 114, no. 12, pp. E2293–E2302, 2017.

[17] P. Loskill, S. G. Marcus, A. Mathur, W. M. Reese, and K. E. Healy, "μorgano: A Lego®-like plug & play system for modular multi-organ-chips," *PLoS One*, vol. 10, no. 10, p. e0139587, 2015.

[18] A. Artzy-Schnirman, N. Hobi, N. Schneider-Daum, O. T. Guenat, C.-M. Lehr *et al.*, "Advanced in vitro lung-on-chip platforms for inhalation assays: From prospect to pipeline," *European Journal of Pharmaceutics and Biopharmaceutics*, vol. 144, pp. 11–17, 2019.

[19] D. E. Ingber, "Human organs-on-chips for disease modelling, drug development and personalized medicine," *Nature Reviews Genetics*, vol. 23, no. 8, pp. 467–491, 2022.

[20] J. P. Wikswo, E. L. Curtis, Z. E. Eagleton, B. C. Evans, A. Kole *et al.*, "Scaling and systems biology for integrating multiple organs-on-a-chip," *Lab on a Chip*, vol. 13, no. 18, p. 3496, 2013.

[21] A. Peirsman, E. Blondeel, T. Ahmed, J. Anckaert, D. Audenaert *et al.*, "MISpheroID: a knowledgebase and transparency tool for minimum information in spheroid identity," *Nature Methods*, vol. 18, no. 11, pp. 1294–1303, 2021.

[22] K. J. Blose, J. T. Krawiec, J. S. Weinbaum, and D. A. Vorp, "Bioreactors for tissue engineering purposes," in *Regenerative Medicine Applications in Organ Transplantation*. Elsevier, 2014, pp. 177–185.

[23] E. Roux, P. Bougaran, P. Dufourcq, and T. Couffinhal, "Fluid shear stress sensing by the endothelial layer," *Frontiers in Physiology*, vol. 11, p. 861, 2020.

[24] B. Davies and T. Morris, "Physiological parameters in laboratory animals and humans," *Pharmaceutical Research*, vol. 10, no. 7, pp. 1093–1095, 1993.

[25] A. Tajeddin and N. Mustafaoglu, "Design and fabrication of organ-on-chips: Promises and challenges," *Micromachines*, vol. 12, no. 12, p. 1443, 2021.

[26] A. Grimmer, W. Haselmayr, and R. Wille, "Automated dimensioning of Networked Labs-on-Chip," *Trans. on Computer-Aided Design of Integrated Circuits and Systems*, pp. 1216–1225, 2018.

[27] H. Bruus, *Theoretical microfluidics*. Oxford university press Oxford, 2008, vol. 18.

[28] M. Takken and R. Wille, "Simulation of pressure-driven and channel-based microfluidics on different abstract levels: A case study," *Sensors*, vol. 22, no. 14, p. 5392.

[29] H. Jasak, "Openfoam: open source CFD in research and industry," *International Journal of Naval Architecture and Ocean Engineering*, vol. 1, no. 2, pp. 89–94, 2009.

[30] R. Vaja and M. Rana, "Drugs and the liver," *Anaesthesia & Intensive Care Medicine*, vol. 21, no. 10, pp. 517–523, 2020.

[31] M. J. Wilmer, C. P. Ng, H. L. Lanz, P. Vulto, L. Suter-Dick *et al.*, "Kidney-on-a-chip technology for drug-induced nephrotoxicity screening," *Trends in Biotechnology*, vol. 34, no. 2, pp. 156–170, 2016.

[32] C. Poon, "Measuring the density and viscosity of culture media for optimized computational fluid dynamics analysis of in vitro devices," *Journal of the Mechanical Behavior of Biomedical Materials*, vol. 126, p. 105024, 2022.

[33] D. C. Fernandes, T. L. Araujo, F. R. Laurindo, and L. Y. Tanaka, "Chapter 7 - hemodynamic forces in the endothelium: From mechanotransduction to implications on development of atherosclerosis," in *Endothelium and Cardiovascular Diseases*, P. L. Da Luz, P. Libby, A. C. Chagas, and F. R. Laurindo, Eds. Academic Press, 2018, pp. 85–95.

[34] J. Bao and D. Jed Harrison, "Measurement of flow in microfluidic networks with micrometer-sized flow restrictors," *AIChE Journal*, vol. 52, no. 1, pp. 75–85.